# Supplementary materials — Anticipating fluctuations of bigeye tuna in the Pacific Ocean from three-dimensional ocean biogeochemistry

Fernando G. Taboada* [1,2], Jong-Yeon Park[3], Barbara A. Muhling[4,5], Desiree Tommasi[4,5], Kisei R. Tanaka[1,6], Ryan R. Rykaczewski[6], Charles A. Stock[2], and Jorge L. Sarmiento [1]

[1]Atmospheric & Oceanic Sciences Program, Princeton University, Princeton, NJ 08540, USA
[2]Geophysical Fluid Dynamics Laboratory, National Oceanic and Atmospheric Administration, Princeton, NJ 08540, USA
[3]Department of Earth and Environmental Sciences, Jeonbuk National University, Jeollabuk-do, 54896, Republic of Korea
[4]Institute for Marine Science, University of California, Santa Cruz, Santa Cruz, CA 95064, USA
[5]National Oceanic and Atmospheric Administration (NOAA), Southwest Fisheries Science Center (SFSC), San Diego, CA 92037, USA
[6]National Oceanic and Atmospheric Administration (NOAA), Pacific Islands Fisheries Science Center (PIFSC), Honolulu, HI 96818, USA

## S1 Supplementary Text

### S1.1 Calculation of $z_{p_{50}}$

Mislan *et al.* [2015] proposed to use the depth of the environmental oxygen pressure resulting in a 50% saturation of whole blood ($z_{p_{50}}$ [m]) to characterize vertical habitat extent for mesopelagic species and used it to project potential changes in the habitat of commercially exploited tuna species due to climate change [Mislan *et al.*, 2017].

The calculation of $z_{p_{50}}$ follows Mislan *et al.* [2015] and it is based on the inversion of van't Hoff equation for the heat of oxygenation, which was parameterized based on experimental estimates by Lowe *et al.* [2000] to retrieve the profile of oxygen binding half saturation at different depths $z$ [m] along the water column;

$$\log p_{50}^{z} = \log p_{50}^{ref} - \frac{1/T_{ref} - 1/T_z}{R} \Delta H'$$

where $\Delta H' = -17\,\mathrm{kJ\,mol^{-1}}$ is the (exothermic) apparent heat of the whole blood-oxygen binding reaction, here for whole blood, and $R = 8.314 \times 10^{-3}\,\mathrm{kJ\,K^{-1}\,mol^{-1}}$ is the universal gas constant. We set $p_{50}^{ref} = 2.12\,\mathrm{kPa}$ as the reference half oxygen saturation at a temperature $T_{ref} = 298.15\,\mathrm{K}$ and for conditions mimicking those of arterial blood in the gills ($0.5\,\%\,CO_2$), based again on Lowe *et al.* [2000] and Mislan *et al.* [2017], but ignoring local acclimation effects. Note also that we are using natural logarithms. We completed the calculation defining $z_{p_{50}}$ as the shallowest depth where ambient $pO_2 \leqslant p_{50}^{z}$, and applying a threshold of 2000 m corresponding to the maximal depth of observed bigeye tuna habitat.

### S1.2 Details about the retrospective forecast experiments

The retrospective forecast experiments provide an initial assessment of the ability of Earth system model predictions to improve the skill of bigeye tuna forecasts. The design parallels the reconstruction of past variability in bigeye tuna abundance, but physical-biogeochemical decade long forecasts [Park *et al.*, 2019] replaced the reanalysis during the forecast period. These forecasts were used to calculate the same annual environmental indices and to project ahead SDMs featuring distinct subsets of indices. Similarly, the goal of the forecast experiments was to assess added skill contributed by physical vs. biogeochemical information, and by surface vs. vertically resolved data for the forecast period. Density dependent effects were dynamically updated based on the previous year forecasts for lead times longer than one year, and the geometric decay in abundance was propagated based on the last available estimate.

As detailed in the text, deviations from a realistic scenario included the use of SDMs trained with data available during the entire study period instead of conducting an online update mimicking how information became available in the past. This choice reflects constraints imposed by the limited duration of the time series relative to low frequency fluctuations identified in our analyses (§3.1) and avoids the computational cost of fitting the comprehensive sequence of GAMs considered

* E-mail: fgtaboada[at]gmail.com, Phone: + 1-609-258-0846, Fax: + 1-609-258-2850
*Present address:* AZTI Marine Research, Basque Research and Technology Alliance (BRTA), Txatxarramendi Ugartea z/g, 48395, Sukarrieta, Spain

herein for a multitude of distinct data combinations. The resulting predictability assessment must be viewed, however, as providing an upper skill bound that may not be reached. We also used all available ECDA-COBALT experiments to estimate the lead dependent climatology that is subtracted from Earth system model forecasts. This procedure removes biases due to model drift towards its own equilibrium once it stops to assimilate observations, although we considered the use of future information here just a minor issue since model drift can be estimated from ensemble simulations. Finally, we applied a lead-dependent climatology to the resulting forecasts and a simple rescaling to mean zero and unit variance to avoid the tendency of SDMs to drift and smooth out variability in bigeye tuna abundance. We also set three year average bigeye tuna abundance as the target of the analyses to match the triennial scale of stock assessments for the fishery.

To assess the extra skill gained by each combination of environmental indices, we focused on the ability of alternative models to reconstruct fluctuations in the overall relative abundance of bigeye tuna in the Pacific. We detrended the resulting series and calculated three year average bigeye tuna abundance to match the triennial scale of stock assessments for the fishery. We projected alternative models starting each year between 1960 and 2017. Models ran into the future for lead times between one and ten years. Predicted abundances were log transformed and averaged over the basin. We then removed the linear trend to retrieve abundance anomalies comparable to those presented in Fig.1. Deviations between forecasts and observed abundances were pooled for different lead times to estimate a series of skill metrics. Skill metrics for each lead time compared aligned pairs of detrended, area-weighted averaged abundance anomalies in the natural log scale. To avoid spurious effects, we sampled the forecasts at the same locations and times as available CPUE data. The declining population trend was independently estimated for the observations and for each SDM forecast, and removed prior to the calculation of the skill metrics.

Anomaly correlations were estimated using Pearson product moment correlations and have a simple interpretation. A high positive correlation suggests that the forecasts has a consistent linear relationship with the observations (*i.e.* qualitatively captures the sign of the response, though it may have a constant, amendable bias). Mean absolute deviations complement the assessment by providing the magnitude of average forecast errors. Lastly, the mean absolute scaled error (MASE), proposed by Hyndman & Koehler [2006], gives the average relative error with respect to a naïve, random walk forecast;

$$q_{t,\tau} = \left| \frac{x_{t,obs} - x_{t,pred}}{\frac{1}{n-1}\sum_{i=\tau}^{n} x_{t,obs} - x_{t-\tau,obs}} \right|$$

where the subscripts *obs* and *pred* refer to observations and forecasts, respectively, and where $\tau$ is the lead time. Values of $\overline{q_t} < 1$ correspond to forecasts beating the benchmark set by the naïve forecast based on the last available observation, providing a simple criteria to judge the overall quality of a forecast.

# References


Hyndman, R.J. & Koehler, A.B. (2006) Another look at measures of forecast accuracy. *International Journal of Forecasting* **22**, 679–688. https://doi.org/10.1016/j.i.jforecast.2006.03.001.

Lowe, T.E., Brill, R.W. & Cousins, K.L. (2000) Blood oxygen-binding characteristics of bigeye tuna (*Thunnus obesus*), a high-energy-demand teleost that is tolerant of low ambient oxygen. *Marine Biology* **136**, 1087–1098. https://doi.org/10.1007/s002270000255.

Mislan, K.A.S., Deutsch, C.A., Brill, R.W., Dunne, J.P. & Sarmiento, J.L. (2017) Projections of climate-driven changes in tuna vertical habitat based on species-specific differences in blood oxygen affinity. *Global Change Biology* **23**, 4019–4028. https://doi.org/10.1111/gcb.13799.

Mislan, K.A.S., Dunne, J.P. & Sarmiento, J.L. (2015) The fundamental niche of blood oxygen binding in the pelagic ocean. *Oikos* **125**, 938–949. https://doi.org/10.1111/oik.02650.

Park, J.Y., Stock, C.A., Dunne, J.P., Yang, X. & Rosati, A. (2019) Seasonal to multiannual marine ecosystem prediction with a global Earth system model. *Science* **365**, 284–288. https://doi.org/10.1126/science.aav6634.

Watanabe, S. (2013) A widely applicable Bayesian information criterion. *Journal of Machine Learning Research* **14**, 867–897.

## S1.3 Supplementary Figures

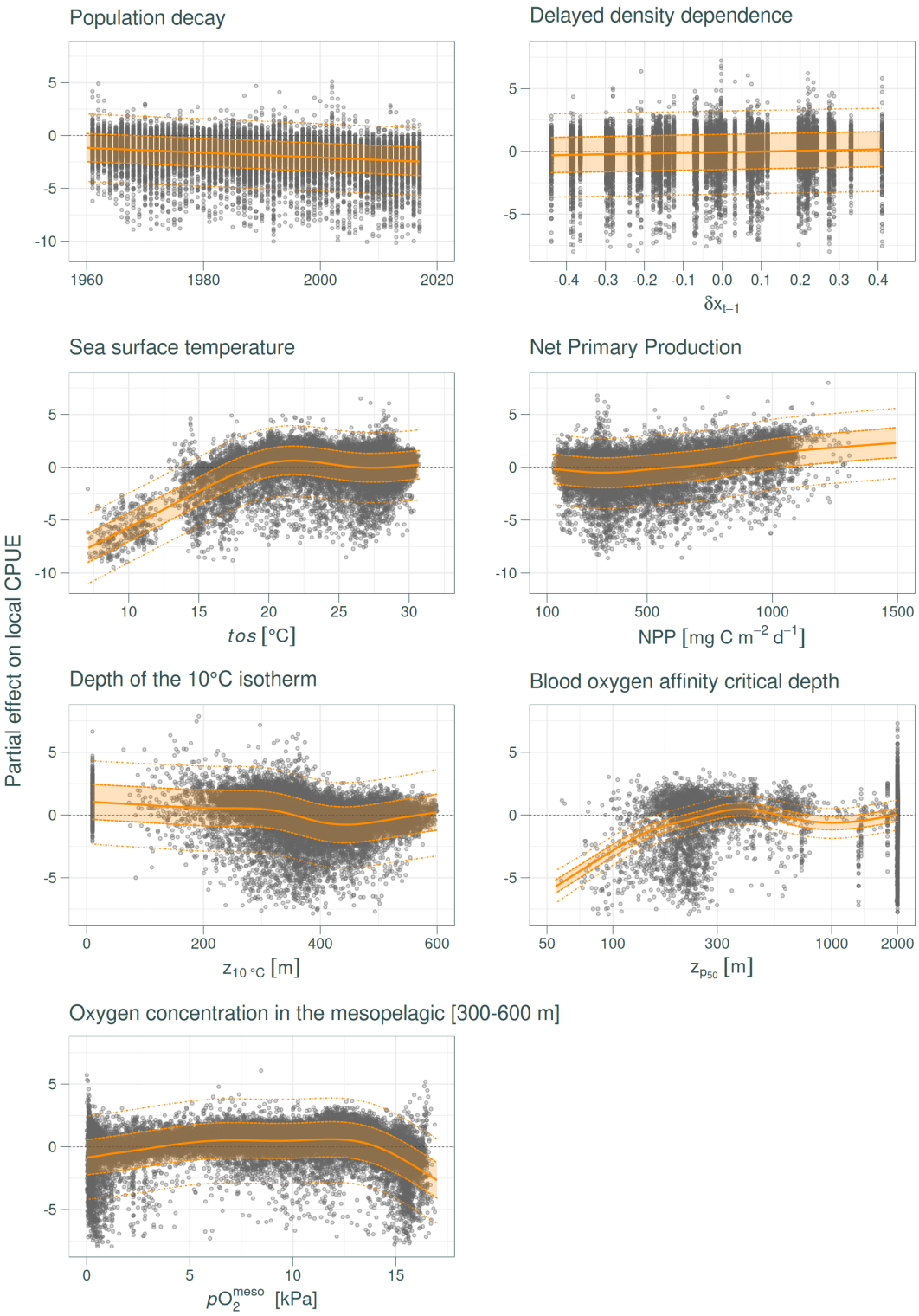


FIGURE S1: Partial effects plot for the saturated model featuring both physical and biogeochemical environmental indices based either on surface or vertically resolved data (*i.e.* model $\mathcal{N}+\mathcal{P}+\mathcal{B}=\mathcal{N}+\mathcal{S}+\mathcal{V}$ in i̇n the main text).

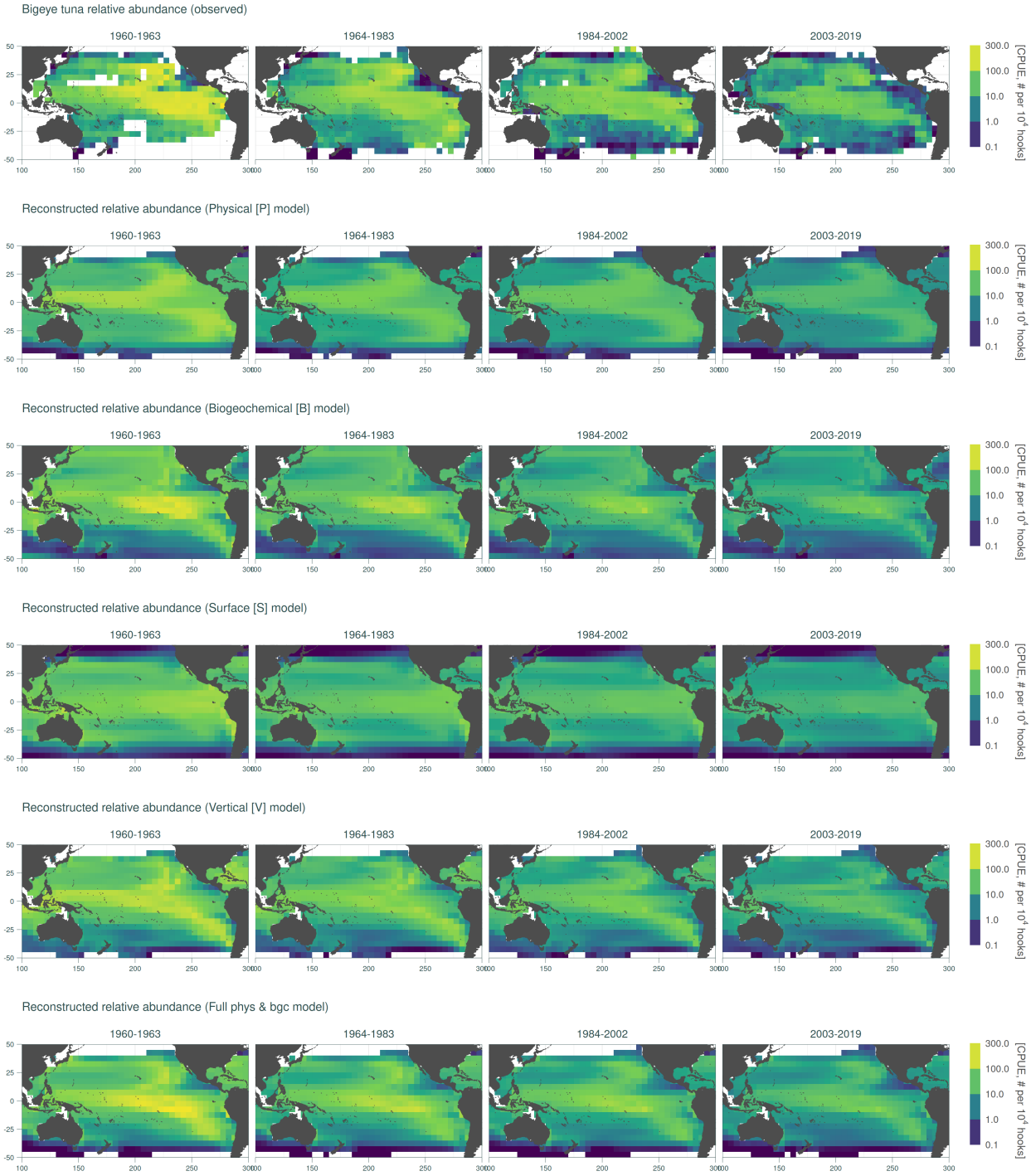


FIGURE S2: Same as Figure 2 in the main text, but featuring the observed and reconstructed changes in bigeye tuna CPUE in the Pacific Ocean, including the downward trend attributed to fishing, during each of the four periods identified using changepoint analysis (Figure 1). The first row of the matrix of maps shows observed patterns, and the other three correspond to reconstructions based on alternative species distribution models (SDMs). CPUE data was based on data retrieved from IATTC and WCPFC databases. As detailed in the main text (see §2.4.2), we considered a series of nested species distribution models (SDMs) of increasing complexity featuring only surface or three-dimensional temperature fields, or vertically resolved biogeochemical information (primary production and oxygen).

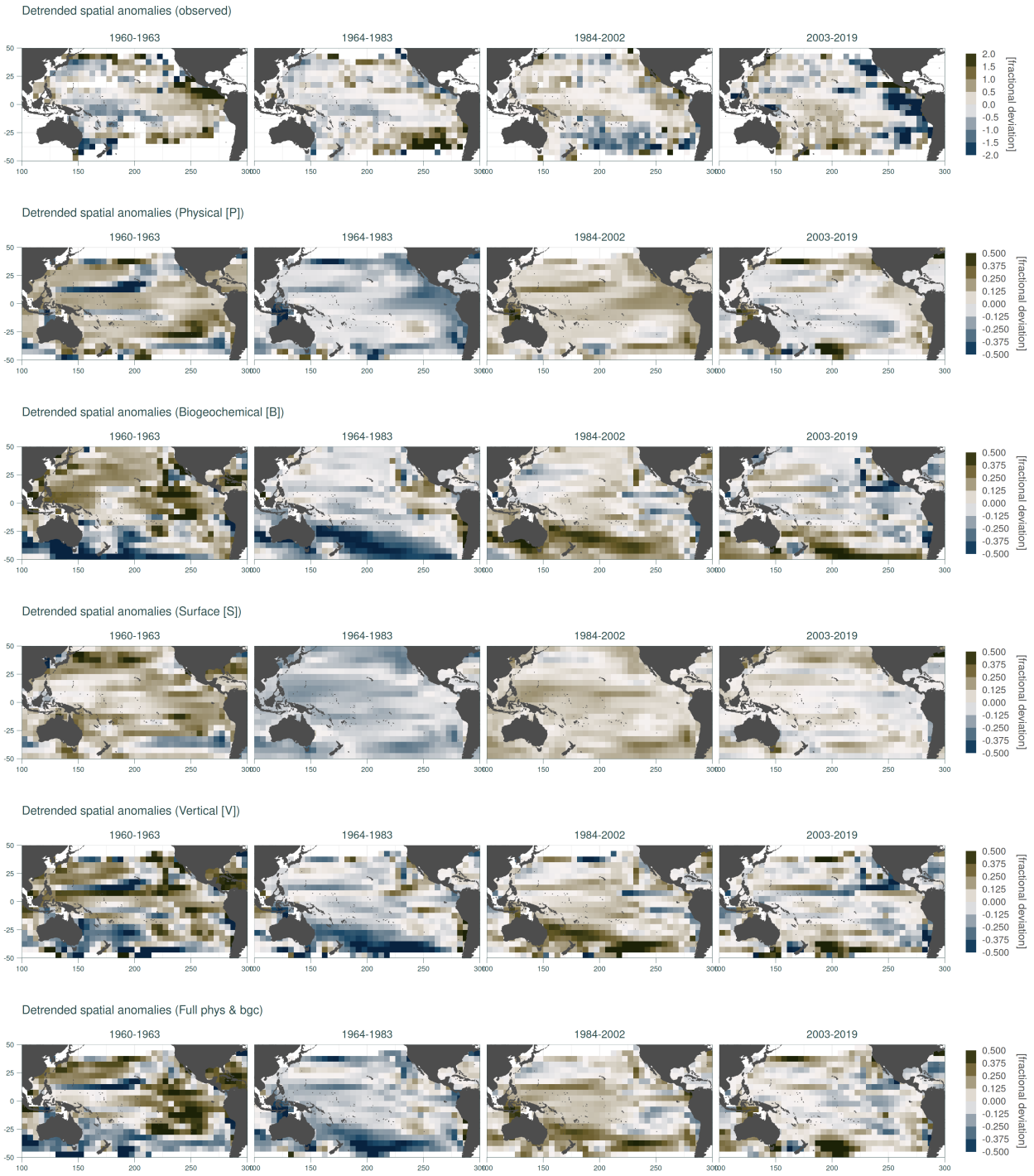


FIGURE S3: Same as Figure 2 in the main text, but featuring observed and reconstructed changes in relative spatial CPUE patterns of bigeye tuna in the Pacific Ocean during each of the four periods identified using changepoint analysis (Figure 1). The first row of the matrix of maps shows observed patterns, and the other three correspond to reconstructions based on alternative species distribution models (SDMs). Anomalies show average deviations during each period from the climatology of linearly detrended deviations of the natural logarithm of CPUE. As detailed in the main text (see §2.4.2), we considered a series of nested species distribution models (SDMs) of increasing complexity featuring only surface or three-dimensional temperature fields, or vertically resolved biogeochemical information (primary production and oxygen). Note the change of scale among the maps featuring spatial anomalies, adjusted to account for the tendency of SDMs to smooth out variability with respect to observations.

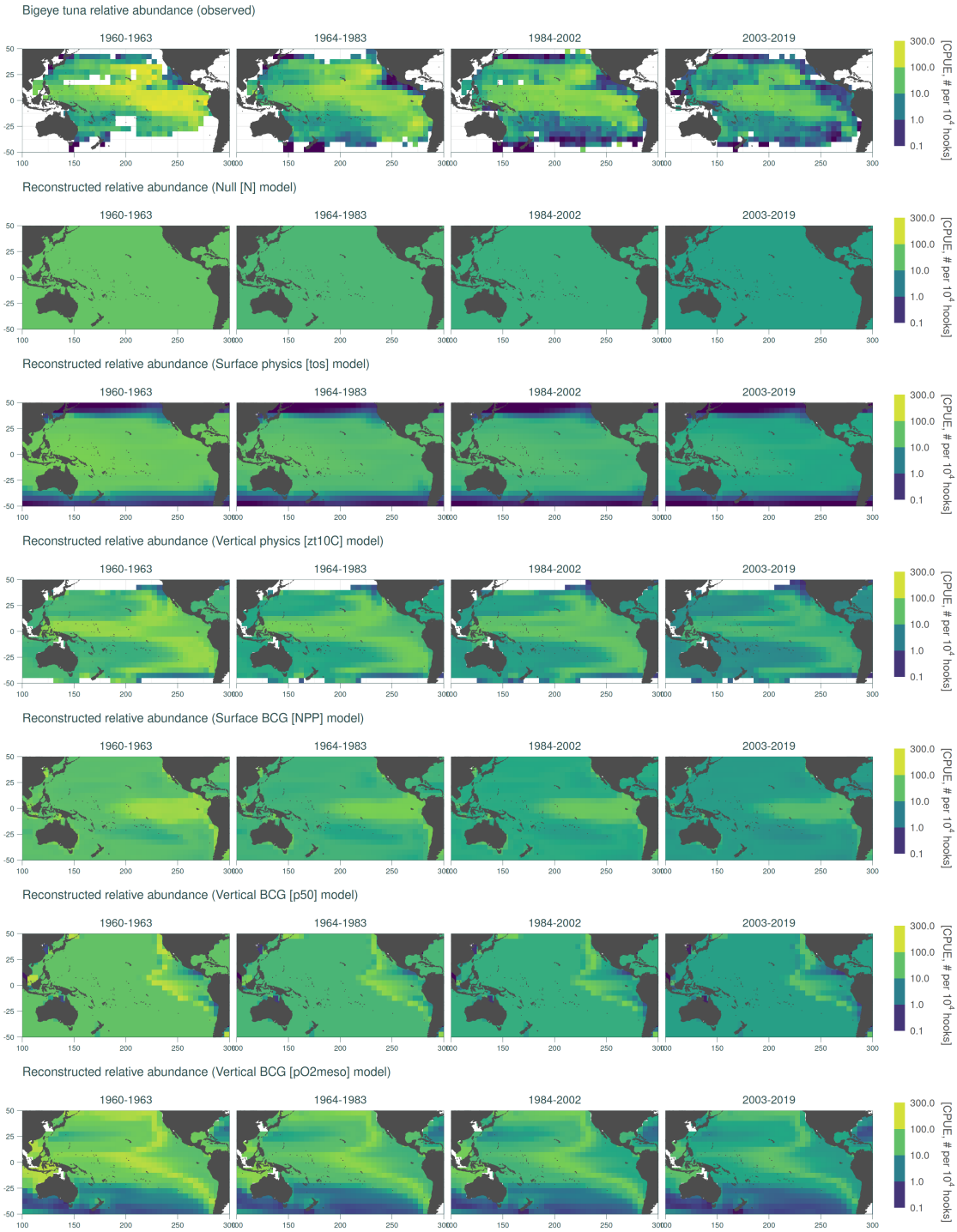


FIGURE S4: Same as Figure S2 above, but comparing observed changes (first row) with reconstructions based on SDMs featuring a single covariate (see the caption of Figure S2 and §2.4.2 in the main text for further details).

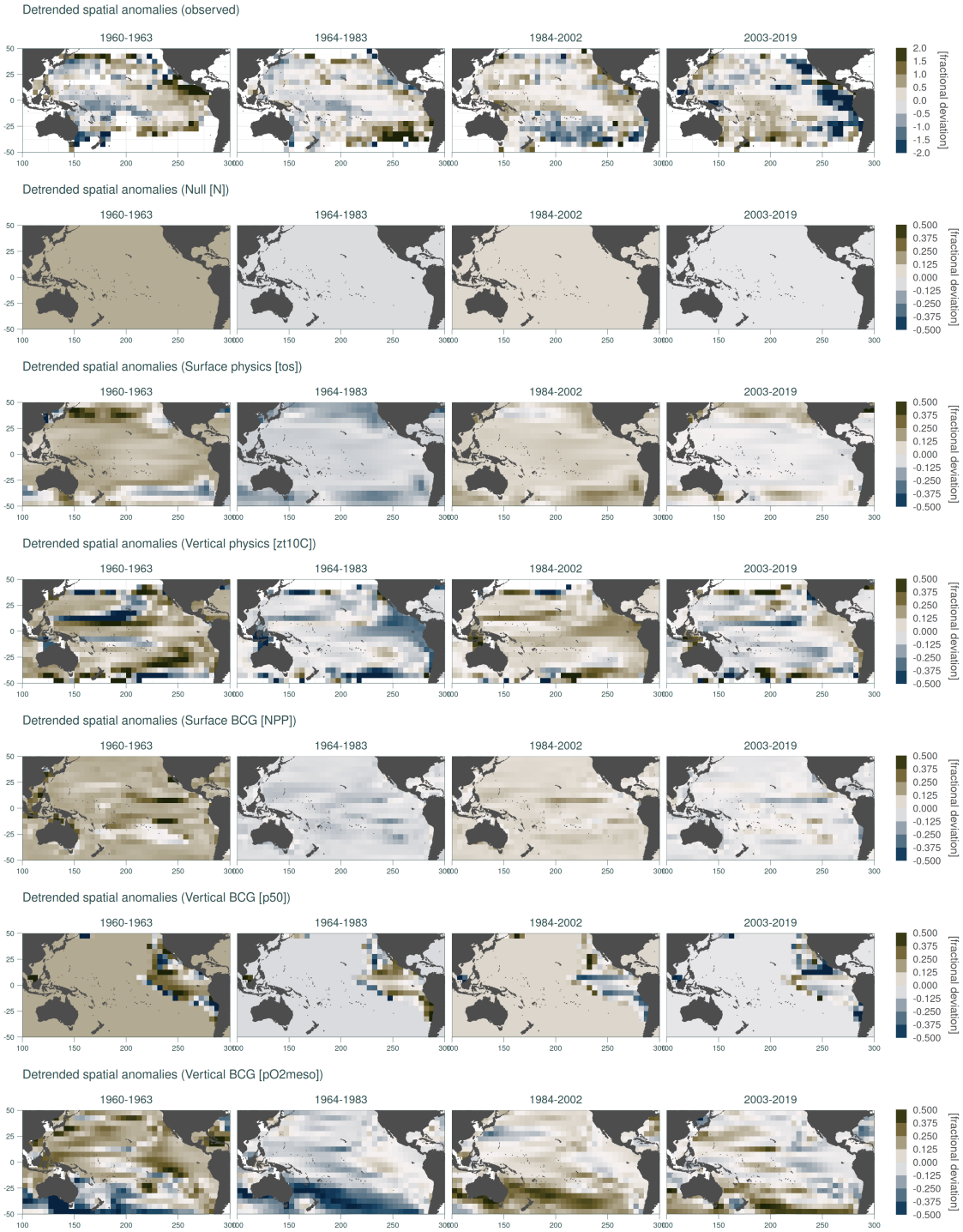


FIGURE S5: Same as Figure S3 above, but comparing observed changes (first row) with reconstructions based on SDMs featuring a single covariate (see the caption of Figure S3 and §2.4.2 in the main text for further details).

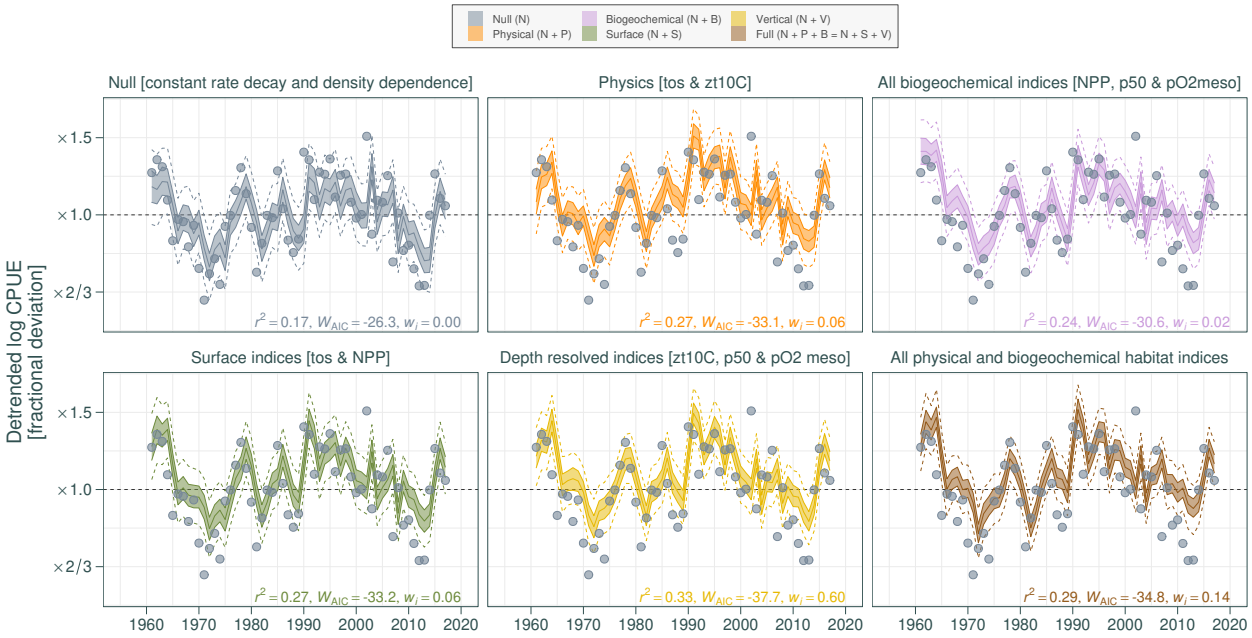


FIGURE S6: Reconstructed, detrended CPUE time series based on posterior simulations the main species distribution models (SDMs) developed to model fluctuations in the abundance of bigeye tuna in the Pacific Ocean between 1955 and 2017. Each model features a different subset of habitat quality indices based on environmental information assimilated using the Earth system model assimilation system ECDA-COBALT. The dots correspond to observations and the lines show the raw series calculated from SDM reconstruction experiments. The ribbon and dashed lines envelope a 50 % and 90 % posterior prediction interval based on 1000 simulations. Each panel further details the $r^2$ as a skill metric and the output of model selection based on Watanabe's [2013] information criterion ($W_{\text{AIC}}$) and their corresponding weights. The assessment compares linear model fits between the observed fluctuations in bigeye tuna abundance and SDM predictions averaged using the same spatial and temporal locations with available observations. We removed the linear trend component from each of the series before the analysis to account for the prominent decay in bigeye tuna abundance due to fishing and avoid spurious relationships. The analysis favored the model $\mathcal{N} + \mathcal{V}$ featuring a constant rate decay and density dependent regulation ($\mathcal{N}$), and the vertically resolved indices ($\mathcal{V}$, *i.e.* the reference isotherm for habitat extent, the isopleth for oxygen saturation of bigeye tuna whole blood, and oxygen concentration in bigeye tuna habitat; see also Table 2 in the main text).

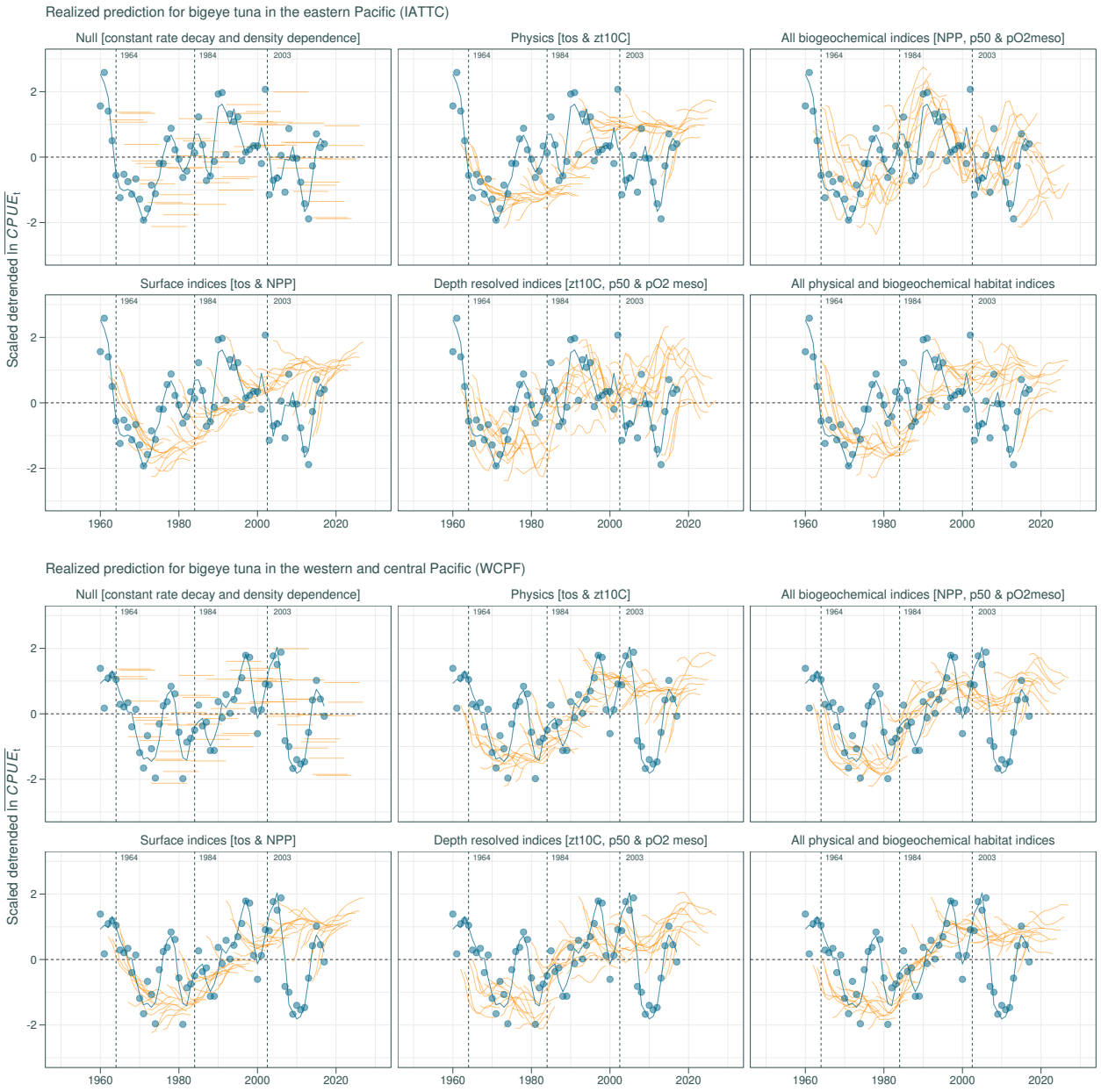


FIGURE S7: Same as Figure 3 in the main text but for the eastern (top) and western (bottom) Pacific. Each panel shows scaled, linearly detrended anomalies in the log transformed CPUE of bigeye tuna, and one to ten year lead forecasts based on different species distribution models and environmental fields forecasted by ECDA-COBALT (see §2.4.3 for further details). The model tends to drift with lead time and to smooth out variabilty in bigeye tuna CPUE, so we subtracted a lead-dependent climatology and a simple centering and rescaling (zero mean, unit standard deviation) to the resulting forecasts. The graph shows scaled CPUE data (*blue dots*); the target, 3-year smoothed series (*blue line*); and 10 year lead forecasts initialized each year between 1961 and 2017 (*orange lines*).

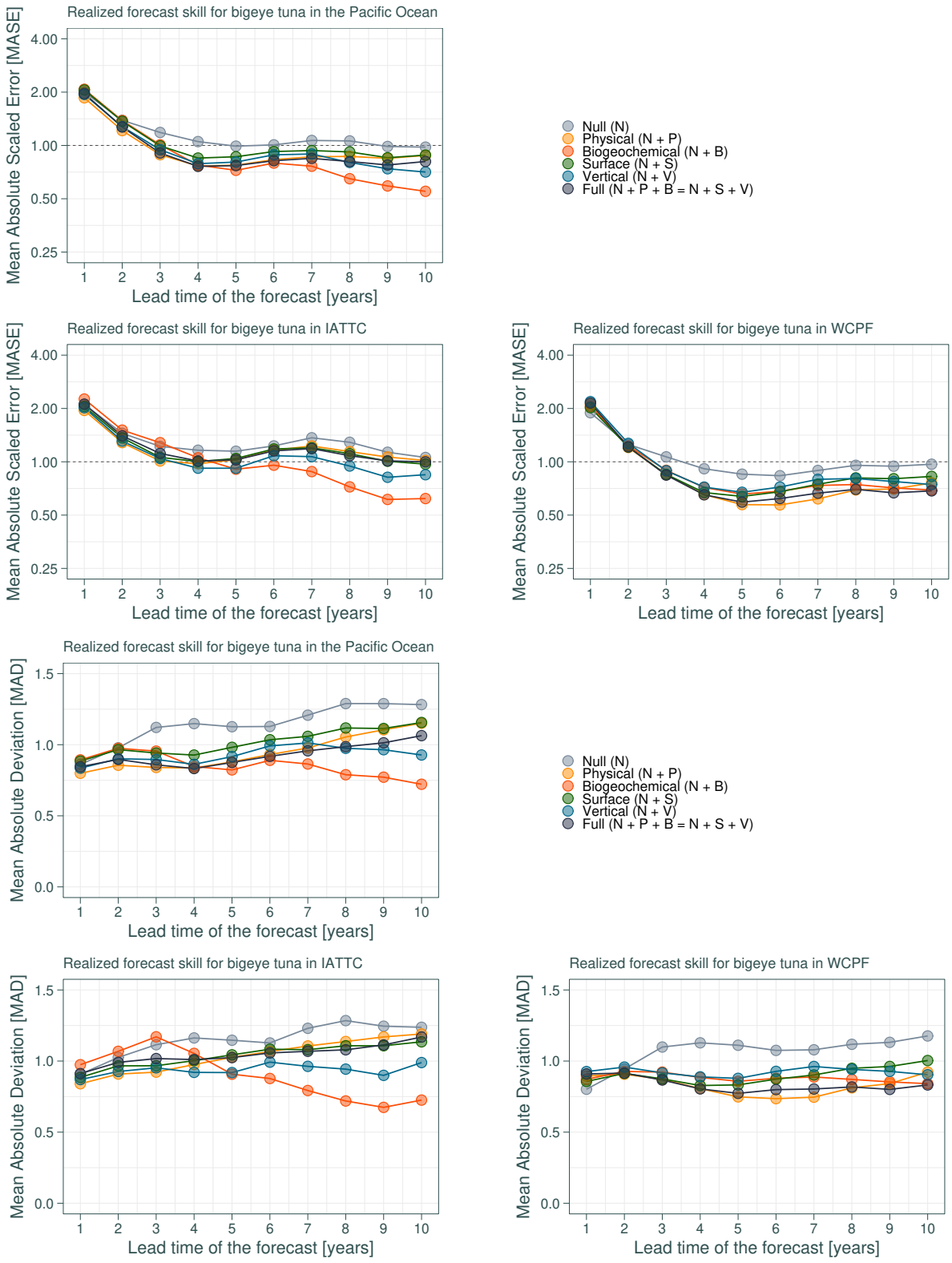


FIGURE S8: Same as Figure 4 in the main text but featuring changes in forecast skill with lead time based on the mean absolute scaled error (MASE) and the mean absolute deviation (MAD) (see §2.4.3 for further details; errors were calculated after applying a lead dependent correction and a simple rescaling to the forecasts).

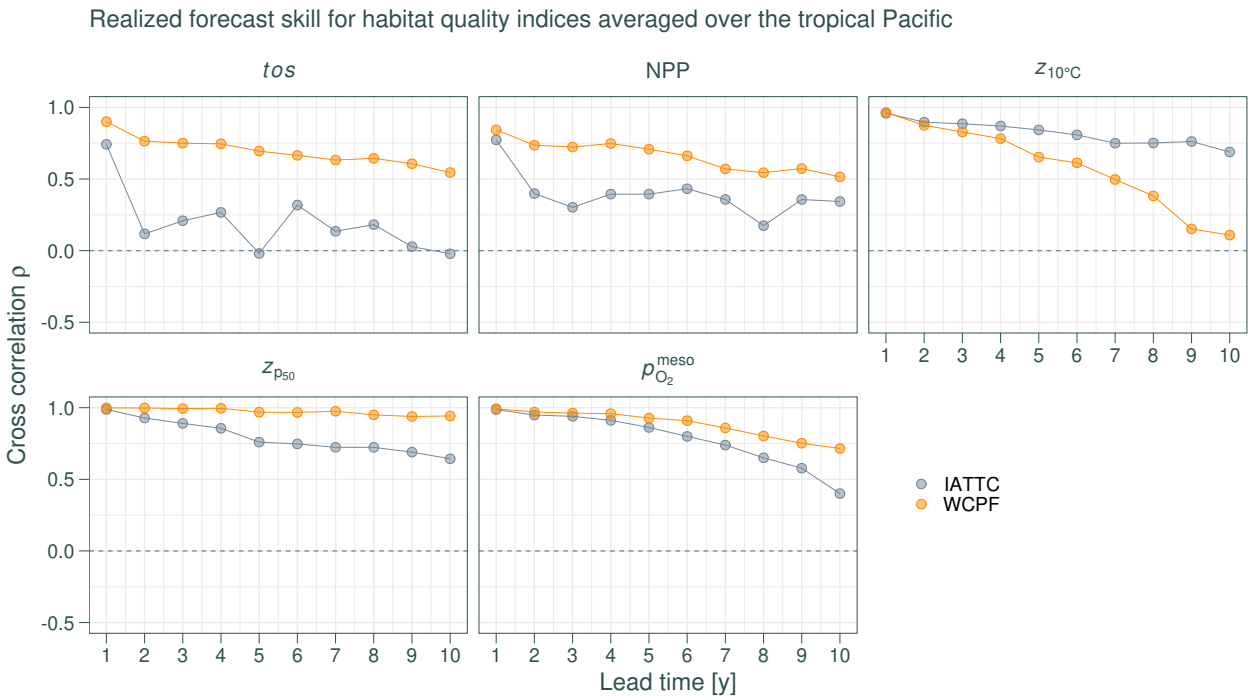


FIGURE S9: Forecast skill at different lead times for habitat quality indices averaged over the eastern and western tropical Pacific Ocean (subset of IATTC and WCPF stock areas between 20°S and 20°*N*) based on ECDA-COBALT decadal experiments (§2.4.3).

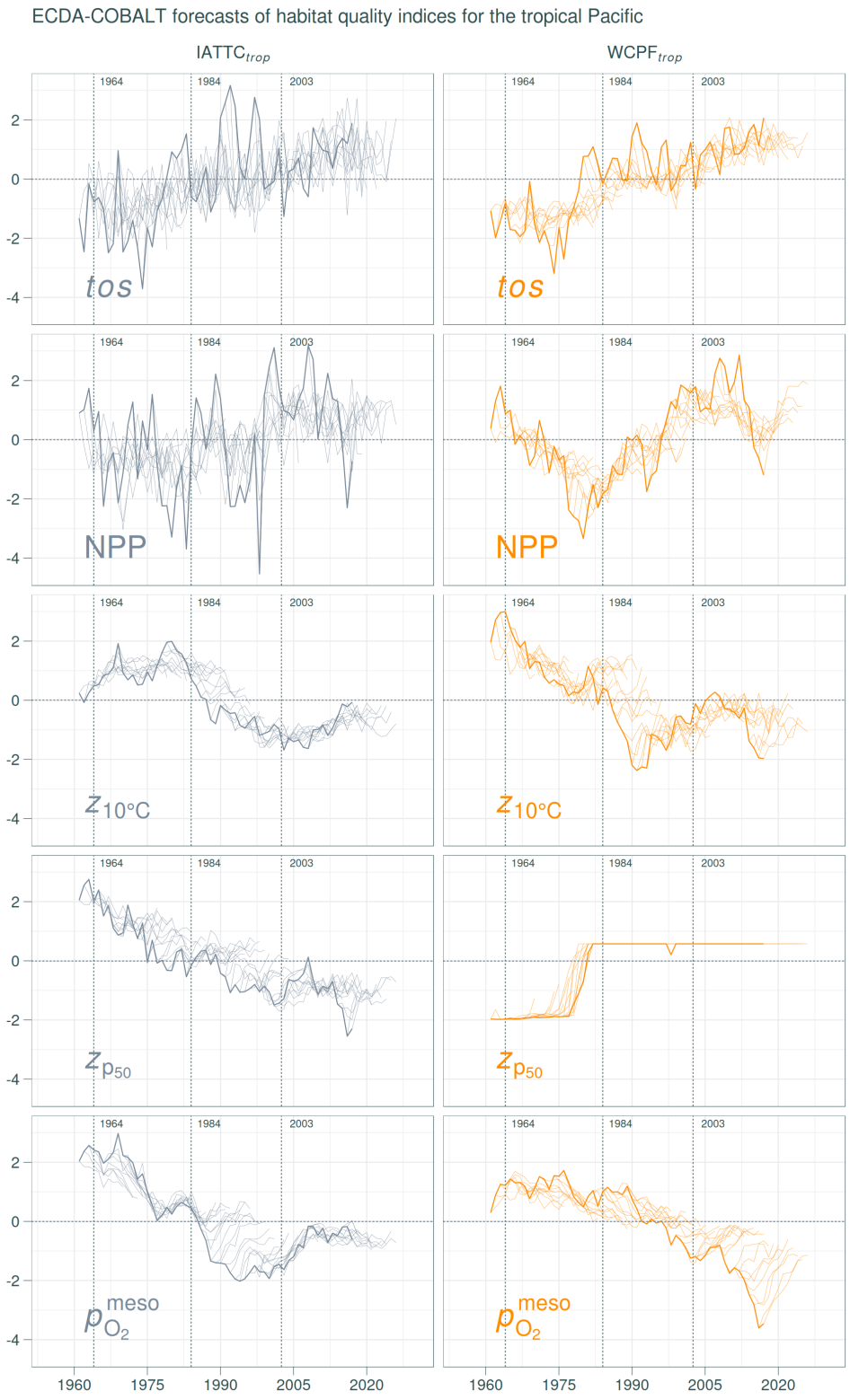


FIGURE S10: Time series forecasts for habitat quality indices averaged over the eastern and western tropical Pacific Ocean (subset of IATTC and WCPF stock areas between 20°S and 20°*N*) based on ECDA-COBALT decadal experiments (§2.4.3). The thick line on each panel corresponds to assimilated states, while the thin lines correspond to each independent decadal experiment. The series were standardized to mean zero and unit variance to ease the comparison between the eastern and westerna Pacific. Please note that, according to ECDA-COBALT and in agreement with observations, areas where $p_{50}$ is below *in situ* saturation were almost limited to the eastern Pacific Ocean. The expansion of anoxic waters towards the west explains the abrupt jump observed in WCPF in 1977.